Model Uncertainty in Cloud–Circulation Coupling, and Cloud-Radiative Response to Increasing CO_2, Linked to Biases in Climatological Circulation

BERNARD R. LIPAT

Department of Applied Physics and Applied Mathematics, Columbia University, New York, New York

AIKO VOIGT

Institute of Meteorology and Climate Research - Department Troposphere Research, Karlsruhe Institute of Technology, Karlsruhe, Germany, and Lamont-Doherty Earth Observatory, Columbia University, Palisades, New York

GEORGE TSELIOUDIS

NASA GISS, and Department of Applied Physics and Applied Mathematics, Columbia University, New York, New York

LORENZO M. POLVANI

Department of Applied Physics and Applied Mathematics, and Department of Earth and Environmental Science, Columbia University, New York, and Lamont-Doherty Earth Observatory, Columbia University, Palisades, New York

(Manuscript received 4 October 2017, in final form 28 June 2018)

ABSTRACT

Recent analyses of global climate models suggest that uncertainty in the coupling between midlatitude clouds and the atmospheric circulation contributes to uncertainty in climate sensitivity. However, the reasons behind model differences in the cloud–circulation coupling have remained unclear. Here, we use a global climate model in an idealized aquaplanet setup to show that the Southern Hemisphere climatological circulation, which in many models is biased equatorward, contributes to the model differences in the cloud–circulation coupling. For the same poleward shift of the Hadley cell (HC) edge, models with narrower climatological HCs exhibit stronger midlatitude cloud-induced shortwave warming than models with wider climatological HCs. This cloud-induced radiative warming results predominantly from a subsidence warming that decreases cloud fraction and is stronger for narrower HCs because of a larger meridional gradient in the vertical velocity. A comparison of our aquaplanet results with comprehensive climate models suggests that about half of the model uncertainty in the midlatitude cloud–circulation coupling stems from this impact of the circulation on the large-scale temperature structure of the atmosphere, and thus could be removed by improving the climatological circulation in models. This illustrates how understanding of large-scale dynamics can help reduce uncertainty in clouds and their response to climate change.

1. Introduction

The large-scale atmospheric circulation and temperature largely determine whether and which clouds form. In turn, clouds impact near and remote atmospheric conditions. This cloud–dynamics–thermodynamics coupling is poorly understood and contributes to uncertainty in how clouds feed back onto climate change (Bony et al. 2015; Voigt and Shaw 2015). Cloud-radiative feedbacks remain the largest source of uncertainty for projections of future climate (Andrews et al. 2012; Vial et al. 2013; Webb et al. 2013; Qu et al. 2014). While it is now believed that the tropical cloud feedback is positive, the sign and strength of the midlatitude cloud feedback remains unclear (Boucher et al. 2013).

Previous work examined the midlatitude shortwave (SW) cloud feedback as a function of dynamics and of thermodynamics. The popular hypothesis, articulated in the Fifth Assessment Report of the International Panel on Climate Change, has been that poleward shifts of the

Supplemental information related to this paper is available at the Journals Online website: https://doi.org/10.1175/JCLI-D-17-0665.s1.

Corresponding author: Bernard R. Lipat, bl2504@columbia.edu

DOI: 10.1175/JCLI-D-17-0665.1

midlatitude eddy-driven jet would result in shortwave warming because clouds would shift to higher latitudes, where a weaker insolation would result in reduced sunlight reflection (Boucher et al. 2013). However, the existence and magnitude of this jet–cloud coupling, and its impact on the shortwave cloud-radiative effect (SWCRE), has been found to depend on ocean basin, season, and climate model (Bender et al. 2012; Grise et al. 2013; Kay et al. 2014; Li et al. 2014; Grise and Polvani 2014; Tselioudis et al. 2016). Not only is the association between poleward jet shifts and the SWCRE highly complex, but other studies have shown that the midlatitude shortwave cloud feedback is associated primarily with thermodynamic, not dynamic, changes (Storelvmo et al. 2015; Kay et al. 2014; Wall and Hartmann 2015). These results have been interpreted to indicate that model biases in clouds and radiation arise from model biases in cloud microphysics, which global models parameterize and for which observations are sparse, and not from biases in large-scale atmospheric dynamics, which models resolve explicitly (Ceppi and Hartmann 2015).

Studies of dynamical controls on midlatitude clouds have almost exclusively focused on the eddy-driven jet. For example, Grise and Polvani (2014) analyze the internal covariability between the jet and SWCRE across the midlatitudes (30°–60°S) in Southern Hemisphere summer (DJF). They find two classes of models among phase 5 of the Coupled Model Intercomparison Project (CMIP5): Type I models exhibit strong midlatitude SW warming with poleward jet shifts, whereas Type II models exhibit only small midlatitude SW changes with poleward jet shifts and agree better with observations than do Type I models. Extending this work, Grise and Medeiros (2016) suggest that the difference in jet–SWCRE covariability between Type I and Type II models lies in different sensitivities of model low clouds to subsidence changes. Increased subsidence on the equatorward flank of the jet in the lower midlatitudes accompanies poleward jet shifts. Low clouds in Type I models are too univariately dependent on this lower-midlatitude vertical velocity compared to low clouds in Type II models and in observations, which depend on estimated inversion strength together with vertical velocity.

Recent observational work, however, shows that midlatitude cloud amount and SWCRE correlate more robustly with the Hadley cell (HC) edge latitude than with the eddy-driven jet latitude (Bender et al. 2012; Tselioudis et al. 2016). Hadley cell dynamics are a convenient bridge between thermodynamics and eddy-driven jet dynamics because subsidence strengthening and subsidence-induced warming accompany poleward HC edge shifts, especially in the lower midlatitudes (Tselioudis et al. 2016; Lipat et al. 2017). In fact, about half of the full shortwave cloud-radiative responses in the lower midlatitudes to $4 \times CO_2$ forcing can be predicted from poleward HC expansion (see Fig. S1 in the online supplemental material) during Southern Hemisphere summer. Further highlighting the importance of the HC for midlatitude clouds and SWCRE, Lipat et al. (2017) demonstrate that differences in the latitude of the climatological HC edge correlate with differences in the midlatitude shortwave cloud-radiative response and with climate sensitivity. Specifically, they found that in CMIP5 models, the climatological HC extent in the Southern Hemisphere is linked to the midlatitude shortwave cloud response to increasing CO_2. With abrupt $4 \times CO_2$ forcing, models with narrower climatological HCs exhibit stronger cloud-induced shortwave warming, which in turn correlates with higher climate sensitivity.

The results of Lipat et al. (2017) clearly suggest that model biases in the HC contribute to model biases in clouds and their radiative effects. Here, we further explore this idea through simulations with a global climate model in which we vary the climatological HC edge but keep the cloud scheme fixed. We show that the weakened midlatitude SWCRE accompanying poleward HC edge shifts depend on the climatological HC edge latitude, consistent with the CMIP5 correlations reported by Lipat et al. (2017), and with similar implications for the SW cloud-radiative response. The model simulations are described in section 2. Our results are presented in section 3. We summarize our conclusions in section 4.

2. Data and methods

We use monthly mean output from the preindustrial (PI) control run (''r1i1p1'') and from the last 50 years of the abrupt $4 \times CO_2$ runs for all available CMIP5 models (Taylor et al. 2012; see also Table S1). We use reanalysis data for the circulation from ERA-Interim (Dee et al. 2011), and satellite retrieval data for the radiative fluxes from ISCCP-FD (Zhang et al. 2004), and for the clouds from ISCCP-D2 (Rossow and Schiffer 1999). We focus on the Southern Hemisphere; because of maximal insolation, we analyze the summer season (DJF). To highlight the cloud–circulation coupling without forcing, we analyze the control runs. We define the HC edge as the latitude of the first zero crossing of the midtropospheric (500 hPa) meridional mass streamfunction. The SWCRE is the difference between the all-sky and clear-sky top-of-atmosphere outgoing solar radiation. To measure the cloud–circulation covariability, we use 1) the HC-SWCRE, defined as the regression at each latitude of the interannual summer-mean time series of the SWCRE onto the HC edge latitude, and

2) the HC-SWCRE index, computed by averaging the HC-SWCRE over a zone 10° poleward and 5° equatorward of each model's climatological HC edge latitude to capture the HC-induced SWCRE changes, although our results are insensitive to the choice of region (see Figs. S2 and S3). This zone, which we refer to as the lower midlatitudes (LML), spans ~30°–45°S in the multimodel mean, similar to the ~28°–48°S zone used by Lipat et al. (2017).

We perform aquaplanet simulations with the ECHAM6 atmosphere general circulation model (Stevens et al. 2013), which is the atmospheric component of the MPI-ESM used for CMIP5 Giorgetta et al. (2013). The model is integrated in T63 resolution (1.875° × 1.875°) with 47 vertical levels and is run for 30 years, excluding the first 10 years of spinup. All boundary conditions are zonally symmetric. Insolation is set to January conditions. We analyze only the summer hemisphere. We introduce artificial Rayleigh drag on the zonal wind u, $\partial_t u = -u/\tau$, in the lower troposphere (between the surface and 700 hPa) to control the position of the climatological HC edge (Chen et al. 2007). The Rayleigh drag maximizes near the surface and decays linearly to zero with decreasing pressure up to 700 hPa. We vary the Rayleigh drag strength τ^{-1} from 0 to 0.5 to 1 to 1.5 to 2.0 day^{-1}. Increasing the drag shifts the HC edge equatorward (Chen et al. 2007). The atmosphere model is coupled to a thermodynamic 10-m slab ocean. The ocean "q flux" for each of the five runs is computed from surface fluxes saved from companion fixed-SST simulations, in which we use the corresponding value of Rayleigh drag and a variant of the Q_{obs}–SST profile (Williamson et al. 2012), shifted 15° latitude southward:

$$T_s(\phi) = \begin{cases} 0°\mathrm{C}, & |\phi| \geq \phi_0 \\ 27°\mathrm{C} \times \left[1 - \frac{1}{2}\sin^2\left(\frac{\pi}{2}\frac{\phi - \phi_{\max}}{\phi_0 + \phi_{\max}}\right) - \frac{1}{2}\sin^4\left(\frac{\pi}{2}\frac{\phi - \phi_{\max}}{\phi_0 + \phi_{\max}}\right)\right], & -\phi_0 < \phi \leq \phi_{\max} \\ 27°\mathrm{C} \times \left[1 - \frac{1}{2}\sin^2\left(\frac{\pi}{2}\frac{\phi - \phi_{\max}}{\phi_0 - \phi_{\max}}\right) - \frac{1}{2}\sin^4\left(\frac{\pi}{2}\frac{\phi - \phi_{\max}}{\phi_0 - \phi_{\max}}\right)\right], & \phi_{\max} < \phi \leq \phi_0 \end{cases}, \quad (1)$$

where $\phi_0 = 60°$ latitude, and $\phi_{\max} = -15°$ latitude. These "q fluxes" act as an idealized ocean circulation and maintain the interactive slab-ocean SSTs close to the fixed-SST values.

3. Results

To motivate this study, we illustrate the CMIP5 model biases in midlatitude clouds, radiation, and dynamics. Using monthly mean output from CMIP5 PI control runs, we present in Fig. 1a the HC-SWCRE, defined as the regression between the interannual zonal-mean SWCRE and the HC edge latitude. From this HC-SWCRE regression, we construct the HC-SWCRE index by averaging the HC-SWCRE regression coefficients over the lower midlatitudes (see section 2). This index, whose magnitude we use to color the models in Fig. 1a, separates models that generally warm with poleward HC edge shifts (positive HC-SWCRE index or "warming" models, in red) from models that generally cool with poleward HC edge shifts (negative HC-SWCRE index or "cooling" models, in blue), similar to the Type I/II classification of Grise and Polvani (2014). All models (except one) display an HC-SWCRE dipole of subtropical (~15°–30°S) cooling and LML (~30°–45°S) warming. As discussed in Lipat et al. (2017), the observations (thick black line in Fig. 1a) do not exhibit an HC-SWCRE dipole, but rather exhibit weak shortwave cloud-radiative cooling throughout the midlatitudes. In the models, little systematic difference exists between the warming and the cooling models in their subtropical HC-SWCRE minima, but the LML HC-SWCRE maxima in the warming models are larger on average than in the cooling models. Furthermore, for the warming models, the HC edge (diamonds in Fig. 1a) is farther equatorward on average than for the cooling models (Lipat et al. 2017), as revealed by the Student's t test ($p = 0.0083$). Hence, we here refer to the warming (cooling) models as narrow (wide) HC models. The overall model spread in the midlatitude HC-SWCRE maxima is about 4 $\mathrm{W\,m^{-2}}$ $(1°)^{-1}$, and the model spread in HC edge latitude is about 7° latitude.

Lipat et al. (2017) have reported a strong correlation between the HC-SWCRE index and the climatological HC edge in CMIP5 models. This correlation suggests that the model bias in clouds and radiation could be linked to the model bias in dynamics. However, since that correlation was derived across different models, it could also arise from intermodel differences, for example, in cloud schemes. To show that that correlation

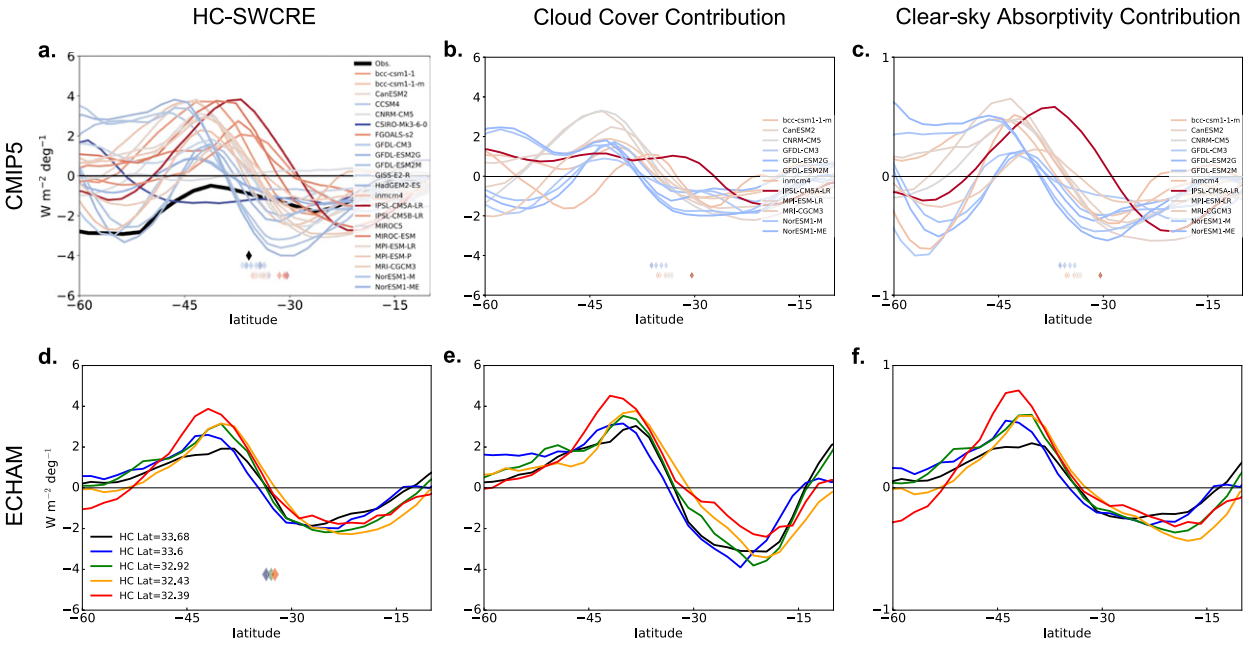

FIG. 1. Impact of HC edge shifts on midlatitude SWCRE. (left) Least squares linear regression coefficients of the zonal-mean SWCRE against the SH HC edge latitude for (a) CMIP5 models where the DJF-mean values are used and (d) the ECHAM6 aquaplanet simulations. The CMIP5 models are red for positive LML HC-SWCRE indices and blue for negative LML HC-SWCRE indices. The ECHAM6 simulations are colored according to their climatological HC edge latitude and LML HC-SWCRE maxima. The diamonds display the climatological HC edge latitude and are colored correspondingly. In (a), the climatological HC edge latitudes of the blue models are displayed above those of the red models for clarity. We display in the thick black line in (a) the observed HC-SWCRE regression derived from ERA-Interim and ISCCP-FD. Decomposition of the full HC-SWCRE regression in (a) and (d) into the (b),(e) SWCRE changes due to cloud cover and (c),(f) changes in clear-sky absorptance using the approximate partial radiative perturbation method of Taylor et al. (2007), for which all CMIP5 data were available. Note the differences in *y*-axis scales across columns.

indeed arises from a systematic impact of the circulation on clouds, we here perform a set of five simulations with the ECHAM6 model (Stevens et al. 2013), used in aquaplanet setup with zonally symmetric Southern Hemisphere summer boundary conditions and coupled to a thermodynamic slab ocean. We introduce different values of boundary layer drag to vary the climatological HC edge between 33.7° and 32.4°S. Figure 1d shows the HC-SWCRE in the five ECHAM6 aquaplanet simulations. Consistent with Lipat et al. (2017), the midlatitude HC-SWCRE maximum is smaller for wide HC cases than for narrow HC cases. With the HC-SWCRE maximum varying by $2\,\mathrm{W\,m^{-2}}\ (1^\circ)^{-1}$ between the five simulations, we can reproduce about half of the CMIP5 model spread in midlatitude HC-SWCRE solely by changing the climatological circulation: the cloud scheme is identical in all five ECHAM6 aquaplanet runs. That is, by pushing the climatological HC toward its observed position, our aquaplanet model exhibits less warming (or Type I) model behavior and more cooling (or Type II) model behavior.

How does the climatological HC latitude affect the cloud–circulation coupling? To answer this question, we use the Taylor et al. (2007) approximate partial radiative perturbation method with a single-layer radiative transfer model, and decompose the HC-SWCRE into contributions from changes in cloud cover, cloud, and clear-sky albedo, and cloud and clear-sky atmospheric absorptivity. For the approximate partial radiative perturbation analysis, we take as the control state the composite of years when the HC edge is anomalously equatorward and as the perturbed state the composite of years when the HC edge is anomalously poleward, normalizing by the difference in HC edge latitude between states. The decomposition (Figs. 1b,c,e,f) reveals that the HC-SWCRE predominantly arises from changes in cloud fraction, with smaller contributions from changes in clear-sky atmospheric absorptivity. This clear-sky absorptivity contribution is likely due to changes in water vapor associated with anomalous subsidence. The impact of cloud albedo and absorptivity (not shown) is two orders of magnitude smaller than that of cloud fraction, indicating that differences in lower-midlatitude HC-SWCRE across both the ECHAM6 simulations and the CMIP5 ensemble do not result from cloud phase changes highlighted in previous studies as important for the cloud-radiative effect at higher latitudes (Ceppi et al. 2014; Ceppi and Hartmann 2015; Wall and Hartmann 2015). Rather, the changes in SWCRE due to HC shifts and those due to thermodynamic

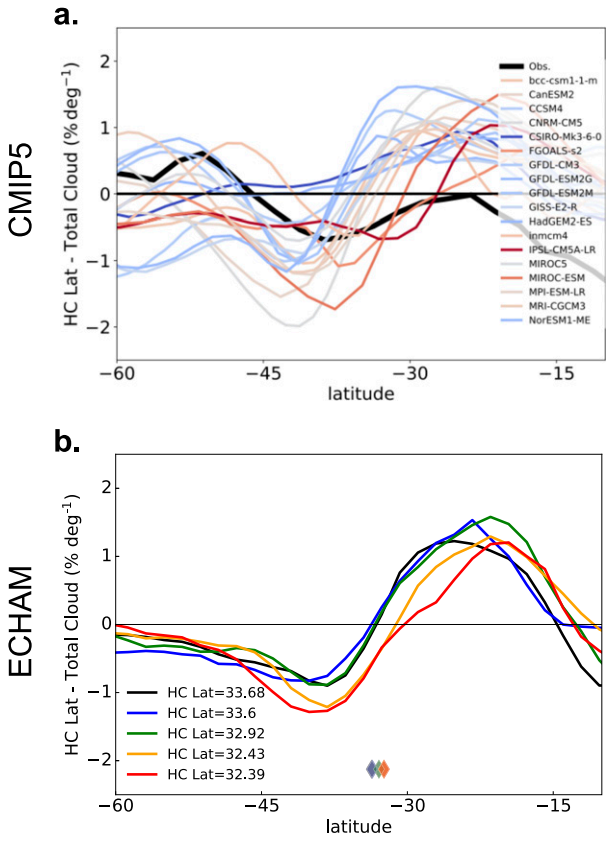

FIG. 2. Midlatitude cloud changes with HC edge shifts. As in Figs. 1a and 1d, but for the least squares linear regression coefficients of the zonal-mean total cloud cover against the SH HC edge latitude for (a) CMIP5 simulations and (b) ECHAM6 models. We display using the thick black line in (a) the observed HC total cloud cover regression derived from ERA-Interim and ISCCP.

phase changes are likely two independent processes that may both be important for the cloud-radiative response to warming.

Figure 2b compares, across the five ECHAM6 simulations, the total cloud cover response to poleward HC edge shifts: one sees that the LML total cloud cover decreases more for narrower HC runs than for wider HC runs. The observations (thick black line in Fig. 2a), on the other hand, exhibit relatively weaker reductions in total cloud cover than in models. The observed decrease in total cloud cover but slight increase in shortwave cloud reflection (thick black line in Fig. 1a) can be explained by a reduction in high cloud but a compensation by low clouds in shortwave reflection (Tselioudis et al. 2016). The ECHAM6 results (Fig. 2b) on the spread in total cloud cover decrease with poleward HC edge shifts and apply to the CMIP5 as well (Fig. 2a): for models with a narrow HC (red lines), one sees more LML cloud cover reduction with poleward HC shifts than for models with a wide HC (blue lines), as revealed by the Student's t test ($p = 0.0433$). Such an association of the LML cloud cover with poleward HC shifts does not exist in the subtropics (15°–30°S), consistent with Figs. 1a and 1d, which shows that the climatological HC edge does not correlate with the magnitude of the subtropical HC-SWCRE minima.

The magnitude of the midlatitude cloud cover reduction with poleward HC shifts is tied to the magnitude of the midlatitude subsidence strengthening accompanying the poleward HC edge shift. To show this, we compare in Fig. 3 the ECHAM6 simulation of the widest HC case (top row) with that of the narrowest HC case (bottom row). We regress on the HC edge latitude the vertical velocity, atmospheric temperature, and relative humidity (left, middle, and right columns of Fig. 3, respectively). The corresponding climatologies are shown with contours, with climatological HC edges denoted by green vertical lines. In both simulations, poleward HC shifts result in stronger midlatitude subsidence, stronger subsidence warming, and reductions in relative humidity. Yet, importantly, all of these responses are larger in the narrowest HC case than in the widest HC case. This is consistent with maximum in warming and in drying that we see in and just above the boundary layers in Fig. 3, although we cannot discount other mechanisms such as boundary layer drying due to free-tropospheric warming (Sherwood et al. 2014). The cloud cover decrease associated with poleward HC shifts is produced by a large-scale relative humidity reduction. It therefore should be qualitatively independent of how a model parameterizes clouds, and should be a robust model behavior.

Having shown that the reduced cloud cover with poleward HC shifts is caused by strengthened subsidence, we now tie the magnitude of that subsidence to the climatological HC edge latitude. Models with wider climatological HCs exhibit weaker midlatitude meridional vertical velocity gradients, and thus smaller subsidence strengthening, smaller warming, and smaller cloud cover reductions for the same poleward HC edge shift than models with narrower climatological HCs. In Fig. 4a, we quantify the relationship between the climatological HC edge and the meridional gradient in vertical velocity that underlies this mechanism. We plot the climatological difference in vertical velocity between 30° and 45°S against the sensitivity of lower-midlatitude mean vertical velocity to poleward HC edge latitude shifts. In both the mid- (500 hPa; dots in Fig. 4a) and lower (775 hPa; stars in Fig. 4a) troposphere, poleward HC edge shifts lead to stronger subsidence in models with larger meridional gradients in vertical velocity. Therefore, across the ECHAM6 simulations, differences in midlatitude HC-SWCRE are linked to differences in the climatological HC edge via the

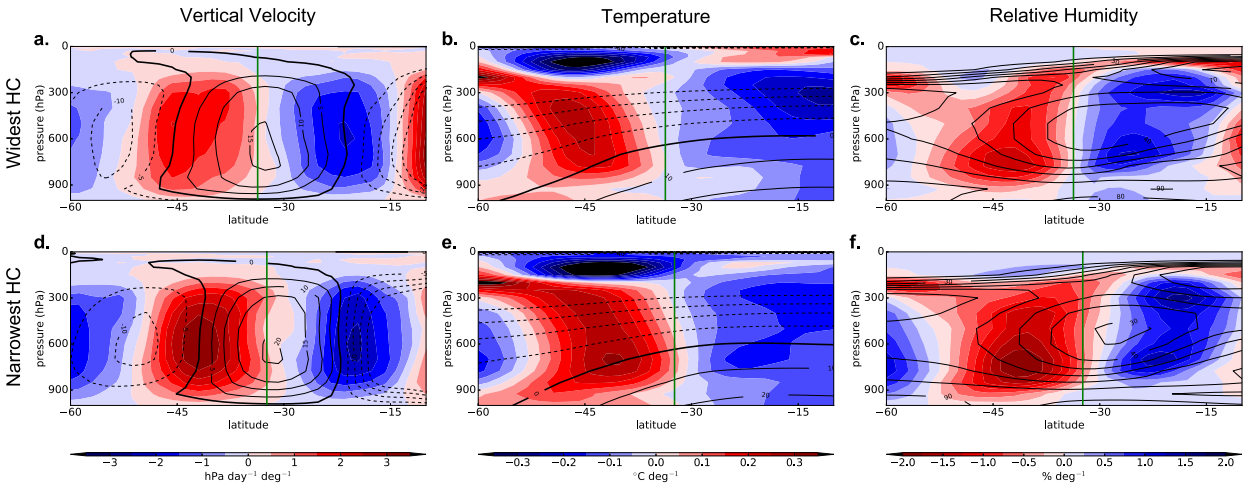

FIG. 3. Dynamic and thermodynamic changes with HC edge shifts. In color shading are the least squares linear regression coefficients of the zonal-mean (left) pressure vertical velocity ω, (center) atmospheric temperature, and (right) relative humidity for the ECHAM6 aquaplanet simulations with the (a)–(c) most poleward (widest) climatological HC edge latitude and (d)–(f) most equatorward (narrowest) climatological HC edge latitude. The climatological HC edge latitude is denoted by a green vertical line. Contours are the corresponding climatological values. In (a) and (d) the 0 hPa day^{-1} contour is thick, and in (b) and (c) the 0°C contour is thick.

connection of the latter to climatological meridional vertical velocity gradients. Again, the ECHAM6 results (Fig. 4a) resemble the biases across CMIP5 models (Fig. 4b). Specifically, the spread across CMIP5 models in the climatological meridional vertical velocity gradients is strongly correlated with the model spread in LML subsidence increase with poleward HC shifts (Fig. 4b dots; correlation coefficient $R = 0.97$) and with the model spread in the HC-SWCRE index (Fig. 4b colors; $R = 0.81$).

4. Conclusions

We have demonstrated that model errors in the simulation of the present-day large-scale atmospheric circulation lead to substantial model errors in how circulation variability impacts midlatitude clouds and their radiative effects. Combining idealized aquaplanet simulations with an analysis of the multimodel CMIP5 ensemble, we have shown that the meridional gradient in midlatitude midtropospheric vertical velocity controls how shifts in the Hadley cell edge impact the midlatitude shortwave cloud-radiative effect. Because the meridional gradient in vertical velocity is strongly tied to the latitude of the climatological Hadley cell edge, we have here identified a mechanism that explains the correlation previously reported in Lipat et al. (2017).

Our results suggest that model biases in the large-scale-circulation climatology influence the midlatitude shortwave cloud-radiative response. We demonstrate this in Fig. 5, where we correlate the model bias in the meridional gradient in vertical velocity with the lower-midlatitude shortwave cloud-radiative response, computed as the $4 \times CO_2$ PI SWCRE in the LML. The strong correlation suggests that the biases in model circulation impact the climate response to forcing. Previous work has argued that differences in the midlatitude cloud-radiative feedback are due primarily to cloud microphysics biases (Kay et al. 2014; Storelvmo et al. 2015; Ceppi and Hartmann 2015). These and our results are not contradictory. First, we examined the SWCRE response in the lower midlatitudes (30°–45°S) to changes in the Hadley circulation, whereas previous work focused on its response in the higher midlatitudes (poleward of 45°S) to changes in the eddy-driven jet. Second, there are two biases to address 1) biases in the sensitivity of small-scale cloud processes to changes in environmental conditions, and 2) biases in how the large-scale circulation and accompanying temperature changes affect clouds. Operating on the large scale via bulk cloud physics, the second bias, which we highlight here, should be independent of small-scale cloud processes.

Unfortunately, it is well established that climate models exhibit persistent biases in the simulation of the large-scale circulation. This is especially true in the Southern Hemisphere, where the midlatitude eddy-driven jet and the Hadley cell edge are too equatorward in most models (e.g., Ceppi et al. 2012). In our aquaplanet simulations, we can show that the closer we push the climatological Hadley cell edge to the observed value, the more realistic the midlatitude SWCRE sensitivity to poleward HC edge shifts becomes. Although the representations of clouds and their radiative effects still need improvement in models, and deficiencies in

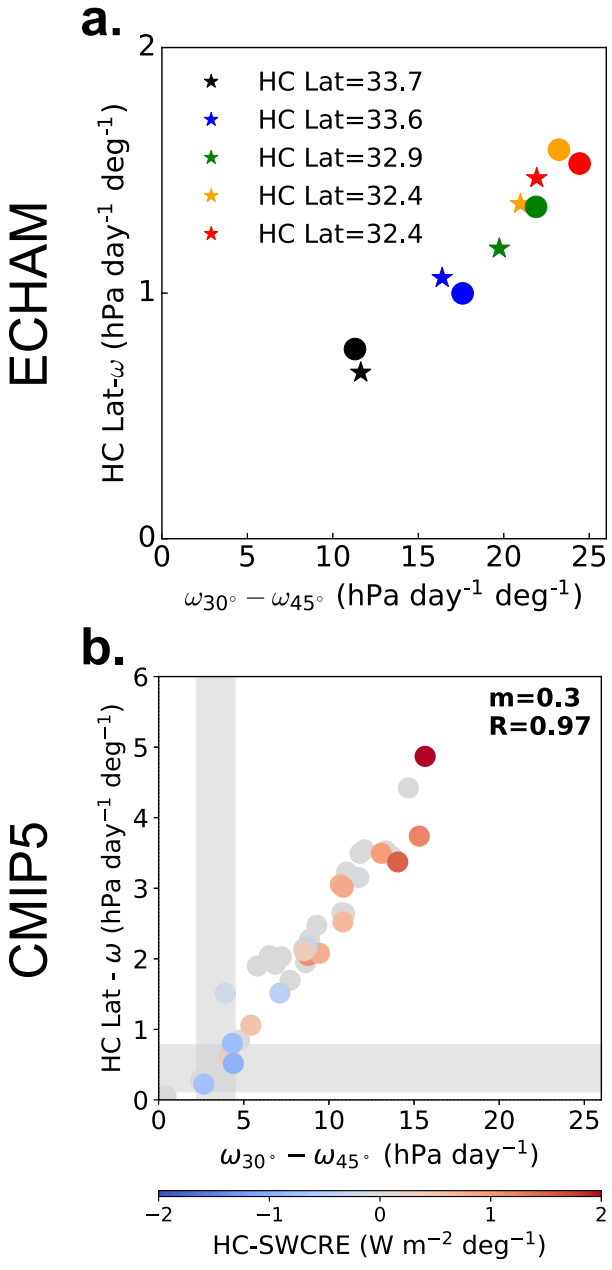

FIG. 4. Relationship between climatological LML meridional vertical velocity gradient and LML subsidence increase with poleward HC shift. Scatterplot of the climatological LML mean pressure vertical velocity (ω) gradient, computed as the difference between ω at 30° and 45°S at 775 hPa (stars) and at 500 hPa (dots) against the least squares linear regression coefficient (HC-ω regression) of the LML mean ω at the corresponding pressure level against the HC edge latitude for (a) each of the ECHAM6 simulations and (b) at 500 hPa for CMIP5 models. The regression coefficient m and correlation coefficient R are displayed. Models are colored according to their HC-SWCRE index, and models without HC-SWCRE data are denoted by gray circles. The 95% confidence interval using the Student's t test on observed values derived from ERA-Interim is denoted by gray shading.

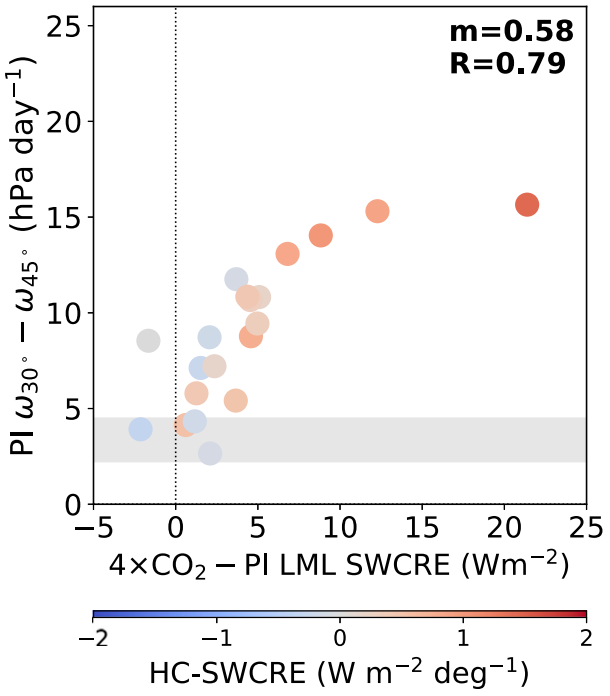

FIG. 5. Relationship between climatological meridional vertical velocity gradient and LML shortwave cloud-radiative response. Scatterplot of the climatological LML (30°–45°S) mean gradient of pressure vertical velocity ω at 500 hPa against the LML shortwave cloud feedback for CMIP5 models. The regression coefficient m and correlation coefficient R are displayed. Models are colored according to their HC-SWCRE index, and models without HC-SWCRE data are denoted by gray circles. The 95% confidence interval using the Student's t test on observed values derived from ERA-Interim is denoted by gray shading.

cloud microphysical schemes must still be addressed, our results offer a promising and perhaps orthogonal way to improve climate models beyond approaches targeting small-scale cloud physics. One such way may involve improved model representations of low-level drag, as highlighted here as well as in, for example, Pithan et al. (2016).

Acknowledgments. We acknowledge the World Climate Research Programme's Working Group on Coupled Modelling, which is responsible for CMIP, and we thank the climate modeling groups for producing and making available their model output. For CMIP, the U.S. Department of Energy's Program for Climate Model Diagnosis and Intercomparison provides coordinating support and led development of software infrastructure in partnership with the Global Organization for Earth System Science Portals. BRL is supported by the NASA Earth and Space Science Fellowship. AV is supported by the German Federal Ministry of Education and Research (BMBF) and FONA: Research for Sustainable Development (www.fona.de) under Grant Agreement

01LK1509A. BRL and GT are supported by NASA MAP. LMP is supported by a National Science Foundation grant to Columbia University.

REFERENCES

Andrews, T., J. M. Gregory, M. J. Webb, and K. E. Taylor, 2012: Forcing, feedbacks and climate sensitivity in CMIP5 coupled atmosphere-ocean climate models. *Geophys. Res. Lett.*, **39**, L09712, https://doi.org/10.1029/2012GL051607.

Bender, F. A.-M., V. Ramanathan, and G. Tselioudis, 2012: Changes in extratropical storm track cloudiness 1983–2008: Observational support for a poleward shift. *Climate Dyn.*, **38**, 2037–2053, https://doi.org/10.1007/s00382-011-1065-6.

Bony, S., and Coauthors, 2015: Clouds, circulation and climate sensitivity. *Nat. Geosci.*, **8**, 261–268, https://doi.org/10.1038/ngeo2398.

Boucher, O., and Coauthors, 2013: Clouds and aerosols. *Climate Change 2013: The Physical Science Basis*, T. F. Stocker et al., Eds., Cambridge University Press, 571–657, https://doi.org/10.1017/CBO9781107415324.016.

Ceppi, P., and D. L. Hartmann, 2015: Connections between clouds, radiation, and midlatitude dynamics: A review. *Curr. Climate Change Rep.*, **1**, 94–102, https://doi.org/10.1007/s40641-015-0010-x.

——, Y.-T. Hwang, D. M. W. Frierson, and D. L. Hartmann, 2012: Southern Hemisphere jet latitude biases in CMIP5 models linked to shortwave cloud forcing. *Geophys. Res. Lett.*, **39**, L19708, https://doi.org/10.1029/2012GL053115.

——, M. D. Zelinka, and D. L. Hartmann, 2014: The response of the Southern Hemispheric eddy-driven jet to future changes in shortwave radiation in CMIP5. *Geophys. Res. Lett.*, **41**, 3244–3250, https://doi.org/10.1002/2014GL060043.

Chen, G., I. M. Held, and W. A. Robinson, 2007: Sensitivity of the latitude of the surface westerlies to surface friction. *J. Atmos. Sci.*, **64**, 2899–2915, https://doi.org/10.1175/JAS3995.1.

Dee, D. P., and Coauthors, 2011: The ERA-Interim reanalysis: Configuration and performance of the data assimilation system. *Quart. J. Roy. Meteor. Soc.*, **137**, 553–597, https://doi.org/10.1002/qj.828.

Giorgetta, M. A., and Coauthors, 2013: Climate and carbon cycle changes from 1850 to 2100 in MPI-ESM simulations for the Coupled Model Intercomparison Project phase 5. *J. Adv. Model. Earth Syst.*, **5**, 572–597, https://doi.org/10.1002/jame.20038.

Grise, K. M., and L. M. Polvani, 2014: Southern Hemisphere cloud–dynamics biases in CMIP5 models and their implications for climate projections. *J. Climate*, **27**, 6074–6092, https://doi.org/10.1175/JCLI-D-14-00113.1.

——, and B. Medeiros, 2016: Understanding the varied influence of midlatitude jet position on clouds and cloud radiative effects in observations and global climate models. *J. Climate*, **29**, 9005–9025, https://doi.org/10.1175/JCLI-D-16-0295.1.

——, L. M. Polvani, G. Tselioudis, Y. Wu, and M. D. Zelinka, 2013: The ozone hole indirect effect: Cloud-radiative anomalies accompanying the poleward shift of the eddy-driven jet in the Southern Hemisphere. *Geophys. Res. Lett.*, **40**, 3688–3692, https://doi.org/10.1002/grl.50675.

Kay, J. E., B. Medeiros, Y. T. Hwang, A. Gettelman, J. Perket, and M. G. Flanner, 2014: Processes controlling Southern Ocean shortwave climate feedbacks in CESM. *Geophys. Res. Lett.*, **41**, 616–622, https://doi.org/10.1002/2013GL058315.

Li, Y., D. W. J. Thompson, Y. Huang, and M. Zhang, 2014: Observed linkages between the northern annular mode/North Atlantic Oscillation, cloud incidence, and cloud radiative forcing. *Geophys. Res. Lett.*, **41**, 1681–1688, https://doi.org/10.1002/2013GL059113.

Lipat, B. R., G. Tselioudis, K. M. Grise, and L. M. Polvani, 2017: CMIP5 models' shortwave cloud radiative response and climate sensitivity linked to the climatological Hadley cell extent. *Geophys. Res. Lett.*, **44**, 5739–5748, https://doi.org/10.1002/2017GL073151.

Pithan, F., T. G. Shepherd, G. Zappa, and I. Sandu, 2016: Climate model biases in jet streams, blocking and stormtracks resulting from missing orographic drag. *Geophys. Res. Lett.*, **43**, 7231–7240, https://doi.org/10.1002/2016GL069551.

Qu, X., A. Hall, S. A. Klein, and P. M. Caldwell, 2014: On the spread of changes in marine low cloud cover in climate model simulations of the 21st century. *Climate Dyn.*, **42**, 2603–2626, https://doi.org/10.1007/s00382-013-1945-z.

Rossow, W. B., and R. A. Schiffer, 1999: Advances in understanding clouds from ISCCP. *Bull. Amer. Meteor. Soc.*, **80**, 2261–2287, https://doi.org/10.1175/1520-0477(1999)080<2261:AIUCFI>2.0.CO;2.

Sherwood, S. C., S. Bony, and J.-L. Dufresne, 2014: Spread in model climate sensitivity traced to atmospheric convective mixing. *Nature*, **505**, 37–42, https://doi.org/10.1038/nature12829.

Stevens, B., and Coauthors, 2013: Atmospheric component of the MPI-M Earth System Model: ECHAM6. *J. Adv. Model. Earth Syst.*, **5**, 146–172, https://doi.org/10.1002/jame.20015.

Storelvmo, T., I. Tan, and A. V. Korolev, 2015: Cloud phase changes induced by CO_2 warming—A powerful yet poorly constrained cloud-climate feedback. *Curr. Climate Change Rep.*, **1**, 288–296, https://doi.org/10.1007/s40641-015-0026-2.

Taylor, K. E., M. Crucifix, P. Braconnot, C. D. Hewitt, C. Doutriaux, J. Broccoli, J. F. B. Mitchell, and M. J. Webb, 2007: Estimating shortwave radiative forcing and response in climate models. *J. Climate*, **20**, 2530–2543, https://doi.org/10.1175/JCLI4143.1.

——, R. J. Stouffer, and G. A. Meehl, 2012: An overview of CMIP5 and the experiment design. *Bull. Amer. Meteor. Soc.*, **93**, 485–498, https://doi.org/10.1175/BAMS-D-11-00094.1.

Tselioudis, G., B. R. Lipat, D. Konsta, K. M. Grise, and L. M. Polvani, 2016: Midlatitude cloud shifts, their primary link to the Hadley cell, and their diverse radiative effects. *Geophys. Res. Lett.*, **43**, 4594–4601, https://doi.org/10.1002/2016GL068242.

Vial, J., J.-L. Dufresne, and S. Bony, 2013: On the interpretation of inter-model spread in CMIP5 climate sensitivity estimates. *Climate Dyn.*, **41**, 3339–3362, https://doi.org/10.1007/s00382-013-1725-9.

Voigt, A., and T. A. Shaw, 2015: Circulation response to warming shaped by radiative changes of clouds and water vapour. *Nat. Geosci.*, **8**, 102–106, https://doi.org/10.1038/ngeo2345.

Wall, C. J., and D. L. Hartmann, 2015: On the influence of poleward jet shift on shortwave cloud feedback in GCMs. *J. Adv. Model. Earth Syst.*, **7**, 2044–2059, https://doi.org/10.1002/2015MS000520.

Webb, M. J., F. H. Lambert, and J. M. Gregory, 2013: Origins of differences in climate sensitivity, forcing and feedback in climate models. *Climate Dyn.*, **40**, 677–707, https://doi.org/10.1007/s00382-012-1336-x.

Williamson, D. L., and Coauthors, 2012: The APE Atlas. NCAR Tech. Note NCAR/TN-484+STR, 508 pp., https://doi.org/10.5065/D6FF3QBR.

Zhang, Y., W. B. Rossow, A. A. Lacis, V. Oinas, and M. I. Mishchenko, 2004: Calculation of radiative fluxes from the surface to top of atmosphere based on ISCCP and other global data sets: Refinements of the radiative transfer model and the input data. *J. Geophys. Res.*, **109**, D19105, https://doi.org/10.1029/2003JD004457.